Dimeric 1,3-propanediaminetetraacetato lanthanides as the precursors of catalysts for the oxidative coupling of methane

Mao-Long Chen, Yu-Hui Hou, Wen-Sheng Xia, Wei-Zheng Weng, Ze-Xing Cao*, Zhao-Hui Zhou*, Hui-Lin Wan

State Key Laboratory of Physical Chemistry of Solid Surfaces, College of Chemistry and Chemical Engineering, Xiamen University, Xiamen, 361005, China, Fax: +86 592 2183047; Tel: +86 592 2184531; E-mail: zxcao@xmu.edu.cn, zhzhou@xmu.edu.cn

Fig. S1 Anion structure of dimeric complex $(NH_4)_2[Ce_2(pdta)_2(H_2O)_4]\cdot 8H_2O$ (**2**) in 30% thermal ellipsoids 2

Fig. S2 Anion structure of dimeric complex $K_2[La_2(pdta)_2(H_2O)_4]\cdot 11H_2O$ (**3**) in 30% thermal ellipsoids 2

Fig. S3 Anion structure of dimeric complex $K_2[Ce_2(pdta)_2(H_2O)_4]\cdot 11H_2O$ (**4**) in 30% thermal ellipsoids 3

Fig. S4 3D supramolecular network of $[La_2(1,3\text{-pdta})_2(H_2O)_4]_n\cdot[Sr_2(H_2O)_6]_n\cdot[La_2(1,3\text{-pdta})_2(H_2O)_2]_n\cdot 18nH_2O$ (**5**) 3

Fig. S5 ^1H NMR spectrum of H_4pdta in D_2O, DSS was used as an internal reference. 4

Fig. S6 ^1H NMR spectrum of $(NH_4)_2[La_2(pdta)_2(H_2O)_4]\cdot 8H_2O$ (**1**) in D_2O, DSS was used as an internal reference. 4

Fig. S7 IR spectrum of $(NH_4)_2[La_2(1,3\text{-pdta})_2(H_2O)_4]\cdot 8H_2O$ (**1**) 5

Fig. S8 IR spectrum of $(NH_4)_2[Ce_2(1,3\text{-pdta})_2(H_2O)_4]\cdot 8H_2O$ (**2**) 5

Fig. S9 IR spectrum of $K_2[La_2(1,3\text{-pdta})_2(H_2O)_4]\cdot 11H_2O$ (**3**) 6

Fig. S10 IR spectrum of $K_2[Ce_2(1,3\text{-pdta})_2(H_2O)_4]\cdot 11H_2O$ (**4**) 6

Fig. S11 IR spectrum of $[La_2(1,3\text{-pdta})_2(H_2O)_4]_n\cdot[Sr_2(H_2O)_6]_n\cdot[La_2(1,3\text{-pdta})_2(H_2O)_2]_n\cdot 18nH_2O$ (**5**) 7

Fig. S12 TG-DTG curves of $(NH_4)_2[La_2(1,3\text{-pdta})_2(H_2O)_4]\cdot 8H_2O$ (**1**) 8

Table S1 The catalytic performances of thermal decomposition products from **1** and **5** in oxidative coupling of methane (CH_4/O_2 = 2.8/1, GHSV = 15000 mL·g^{-1}·h^{-1})..9

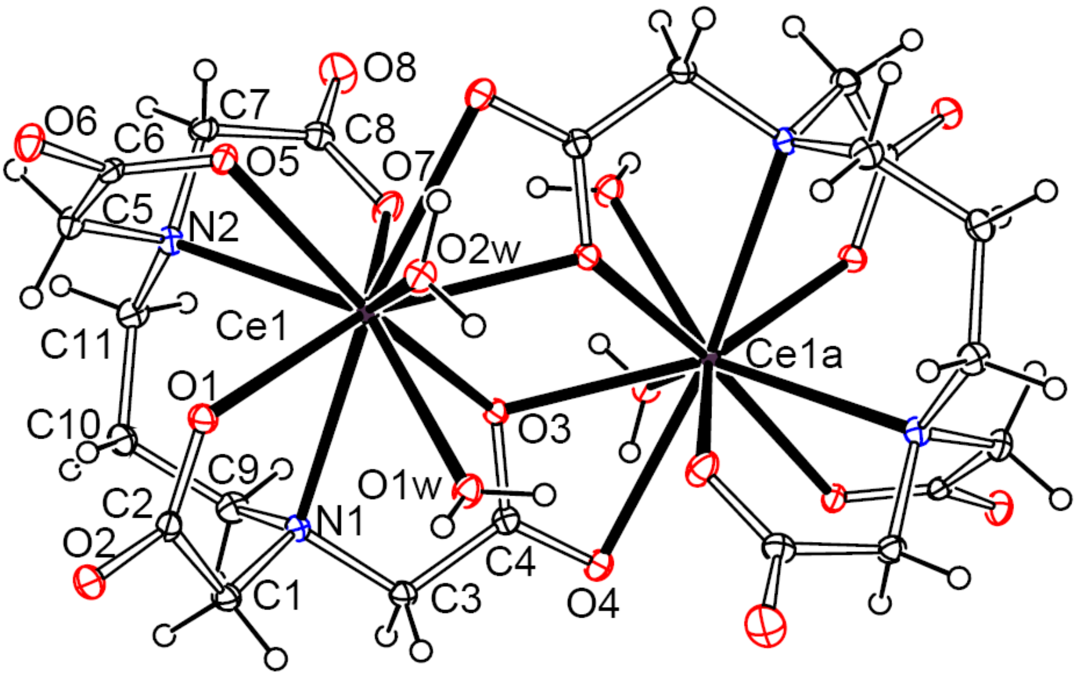

Fig. S1 Anion structure of dimeric complex $(NH_4)_2[Ce_2(pdta)_2(H_2O)_4]\cdot 8H_2O$ (**2**) in 30% thermal ellipsoids

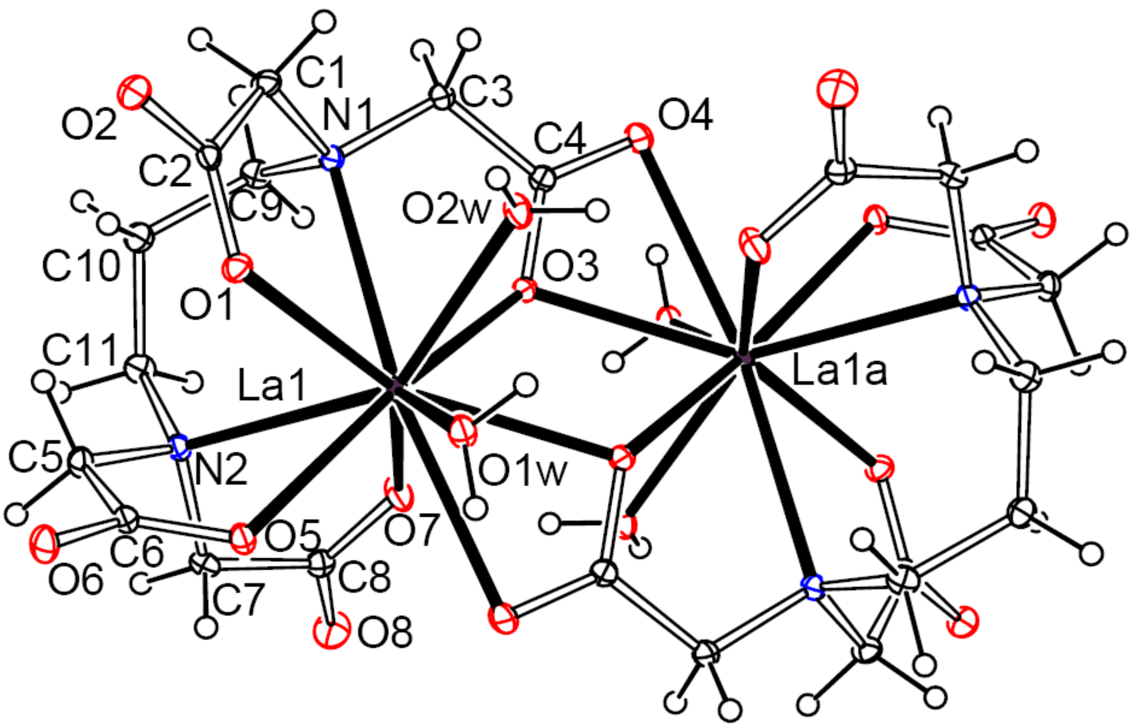

Fig. S2 Anion structure of dimeric complex $K_2[La_2(pdta)_2(H_2O)_4]\cdot 11H_2O$ (**3**) in 30% thermal ellipsoids

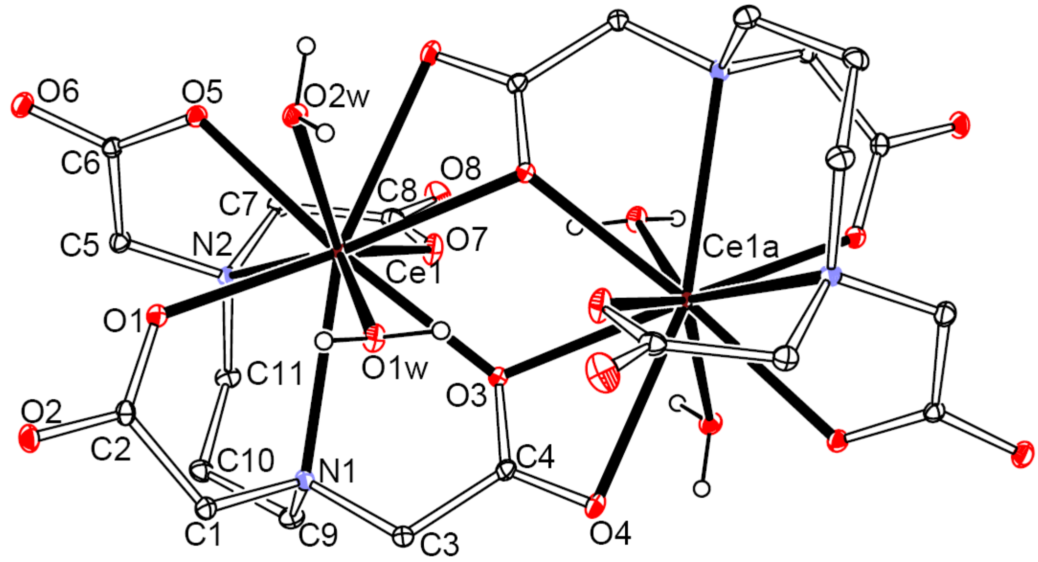

Fig. S3 Anion structure of dimeric complex $K_2[Ce_2(pdta)_2(H_2O)_4]\cdot 11H_2O$ (**4**) in 30% thermal ellipsoids

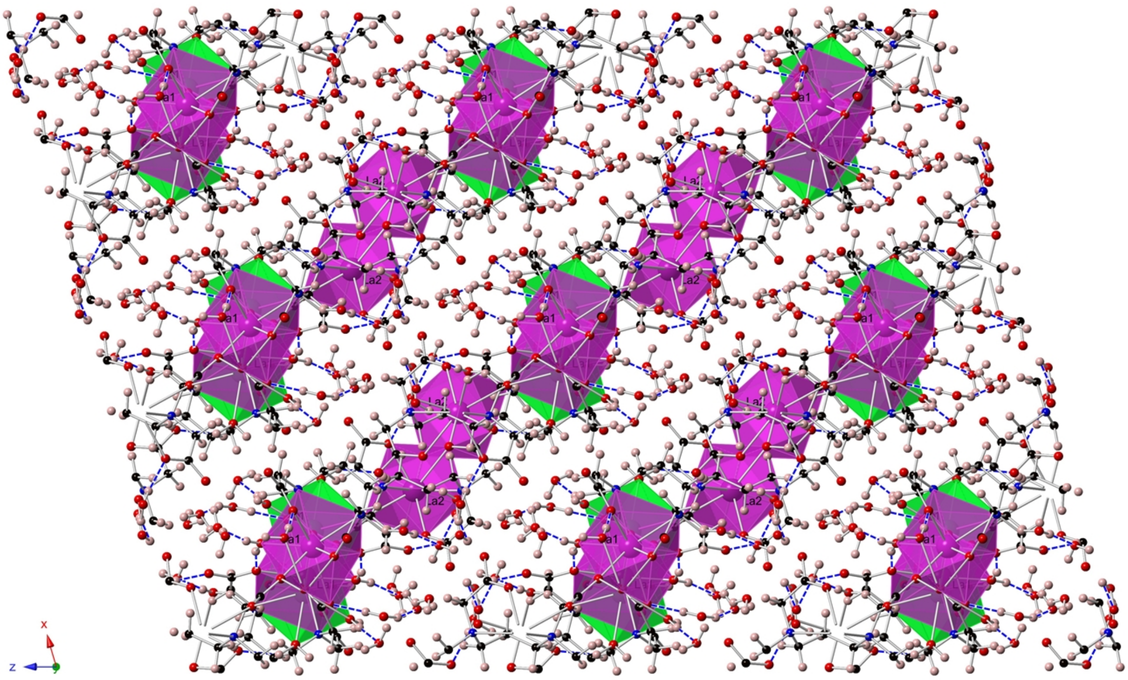

Fig. S4 3D supramolecular network of $[La_2(1,3\text{-pdta})_2(H_2O)_4]_n\cdot[Sr_2(H_2O)_6]_n\cdot[La_2(1,3\text{-pdta})_2(H_2O)_2]_n\cdot 18nH_2O$ (**5**)

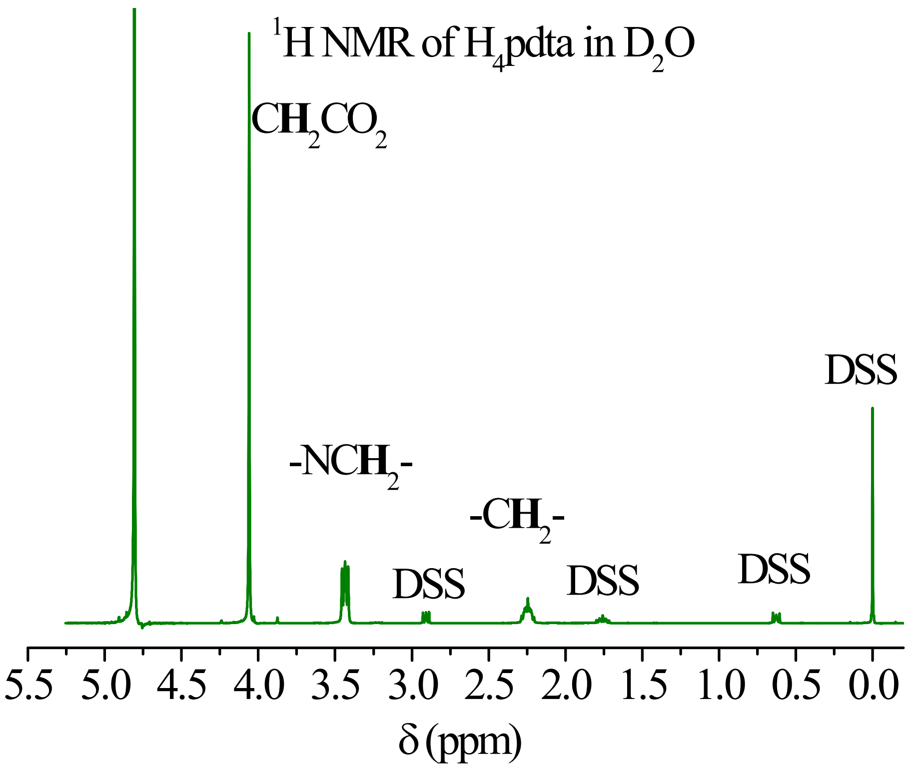

Fig. S5 ^{1}H NMR spectrum of H_4pdta in D_2O, DSS was used as an internal reference.

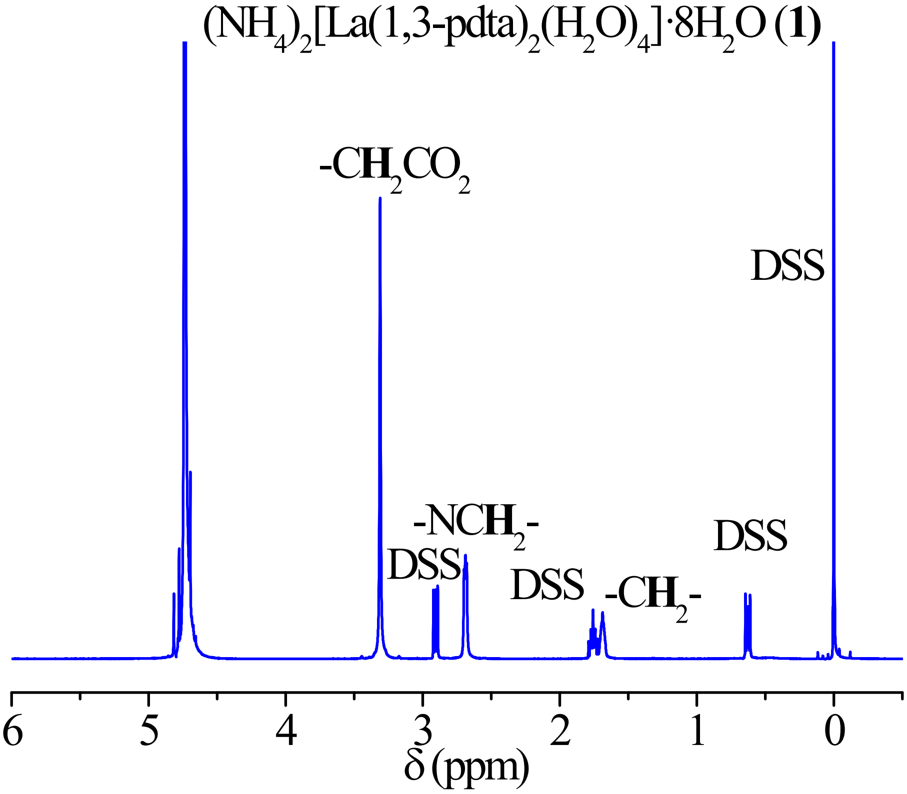

Fig. S6 ^1H NMR spectrum of $(NH_4)_2[La_2(pdta)_2(H_2O)_4]\cdot 8H_2O$ (**1**) in D_2O, DSS was used as an internal reference.

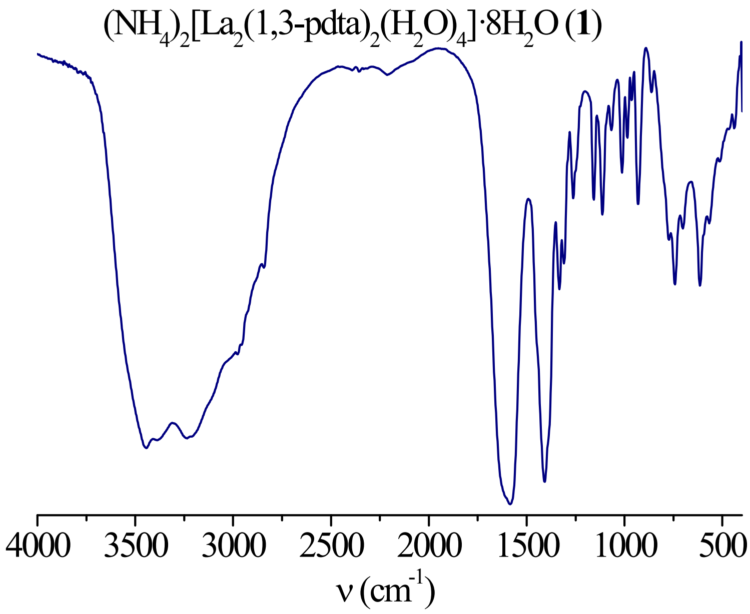

Fig. S7 IR spectrum of $(NH_4)_2[La_2(1,3\text{-pdta})_2(H_2O)_4]\cdot 8H_2O$ (**1**)

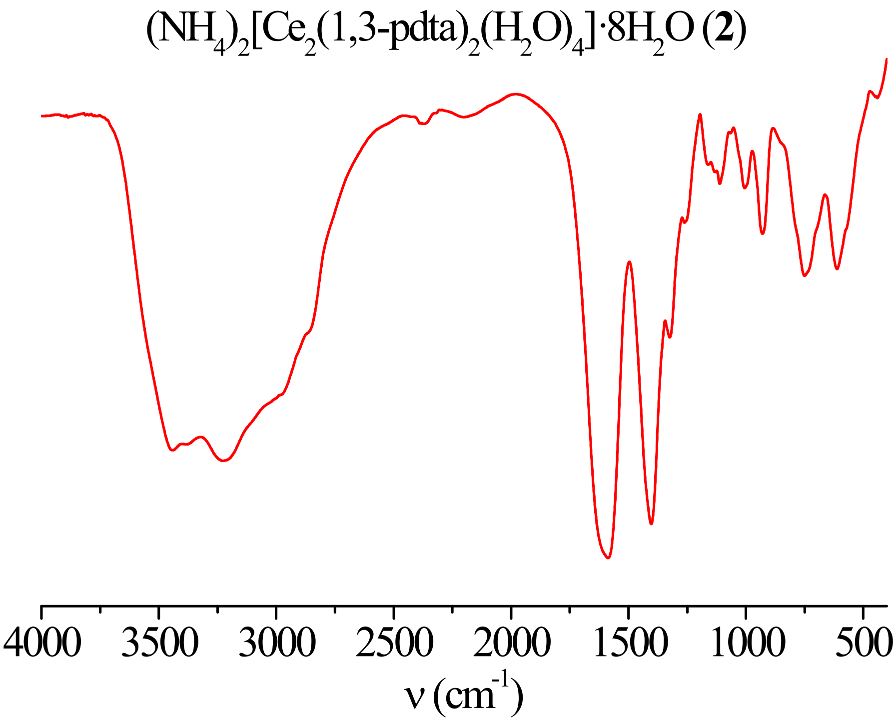

Fig. S8 IR spectrum of $(NH_4)_2[Ce_2(1,3\text{-pdta})_2(H_2O)_4]\cdot 8H_2O$ (**2**)

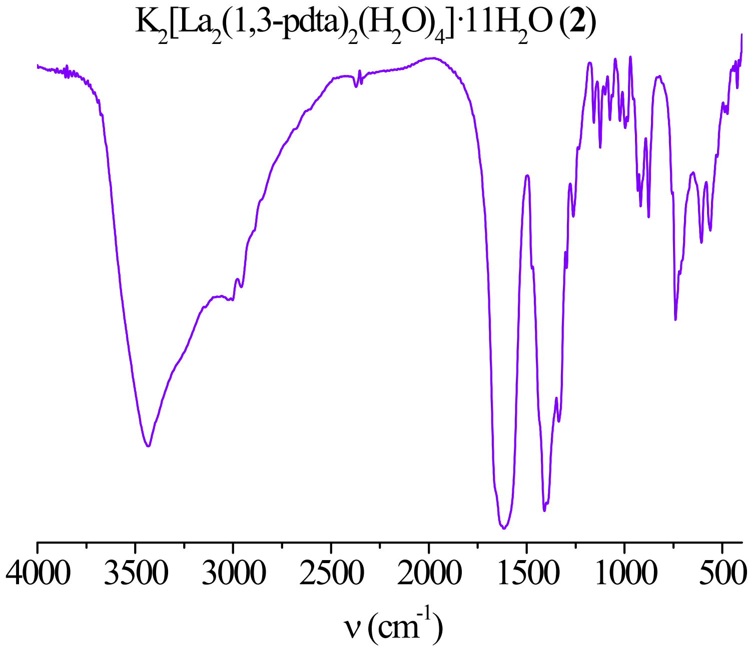

Fig. S9 IR spectrum of $K_2[La_2(1,3\text{-pdta})_2(H_2O)_4]\cdot 11H_2O$ (**3**)

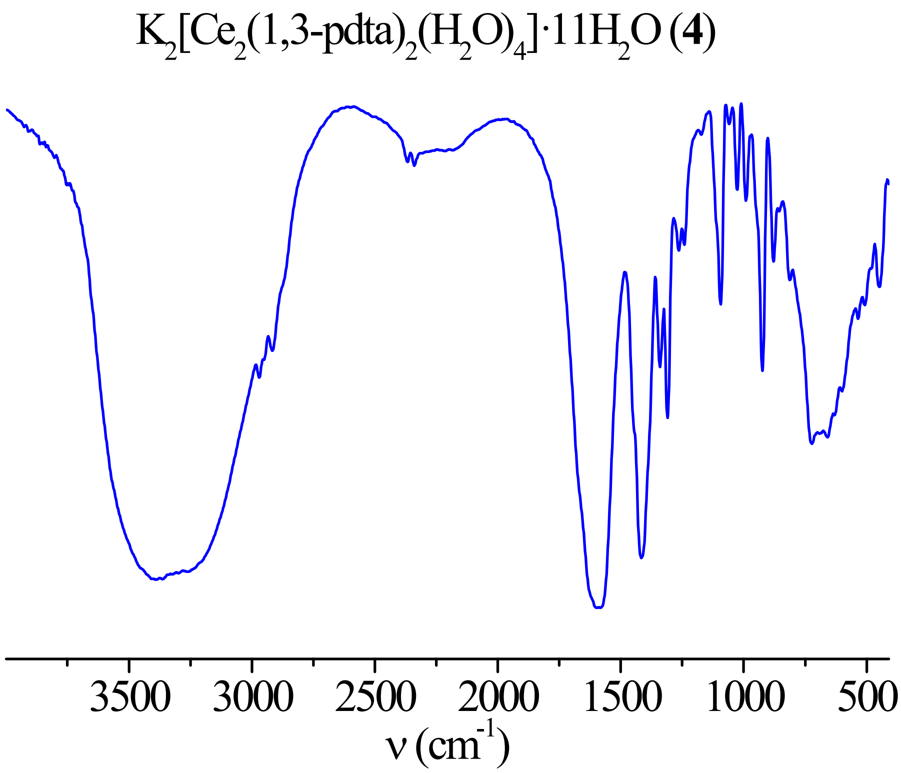

Fig. S10 IR spectrum of $K_2[Ce_2(1,3\text{-pdta})_2(H_2O)_4]\cdot 11H_2O$ (**4**)

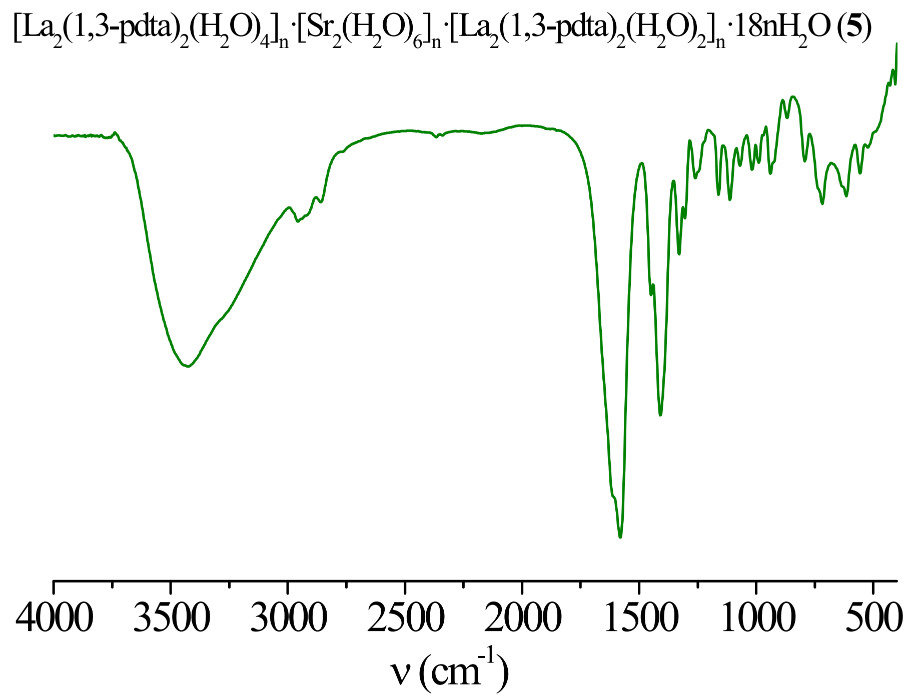

Fig. S11 IR spectrum of $[La_2(1,3\text{-pdta})_2(H_2O)_4]_n\cdot[Sr_2(H_2O)_6]_n\cdot[La_2(1,3\text{-pdta})_2(H_2O)_2]_n\cdot 18nH_2O$ (**5**)

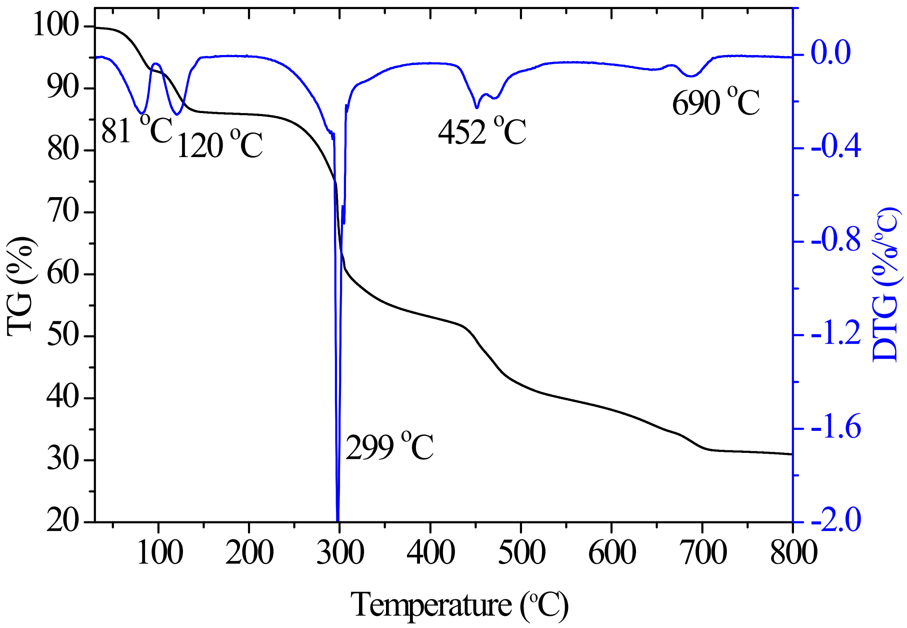

Fig. S12 TG-DTG curves of $(NH_4)_2[La_2(1,3\text{-pdta})_2(H_2O)_4]\cdot 8H_2O$ (**1**)

Table S1 The catalytic performances of thermal decomposition products from **1** and **5** in oxidative coupling of methane (CH_4/O_2 = 2.8/1, GHSV = 15000 mL·g^{-1}·h^{-1})

Sample	T/°C	Conv CH_4/%	Sel C_2/%	Yield C_2/%
$La_2O_2CO_3$	550	0.0	0.0	0.0
	600	13.10	28.38	3.72
	650	17.36	42.37	7.35
	700	23.02	45.75	10.53
	750	29.62	46.57	13.79
	800	29.93	45.61	13.65
La_2O_3, $SrCO_3$ and $La_2O_2CO_3$	550	12.63	24.05	3.04
	600	26.46	47.17	12.48
	650	29.87	46.31	13.83
	700	29.09	50.25	14.62
	750	29.69	51.74	15.36
	800	30.94	50.71	15.69